Yttria-Stabilized Zirconia Assisted Green Electrochemical Preparation of Silicon from Solid Silica in Calcium Chloride Melt

YUNMING GAO,[1,2,*] ZHENBIAO HUANG,[1,2] LIN HE,[1,2] GEORGE Z. CHEN,[1,2,3] QINGWEI QIN,[1,2] and GUANGQIANG LI[1,2]

1. The State Key Laboratory of Refractories and Metallurgy, Wuhan University of Science and Technology, Wuhan 430081, China.
2. Key Laboratory for Ferrous Metallurgy and Resources Utilization of Ministry of Education, Wuhan University of Science and Technology, Wuhan 430081, China.
3. Department of Chemical and Environmental Engineering, Faculty of Engineering, University of Nottingham, Nottingham NG7 2RD, UK.

*Corresponding Author E-mail: gaoyunming@wust.edu.cn

ABSTRACT

A novel integrated cell with O^{2-}|YSZ|Pt|O_2(air) reference and counter electrodes was constructed using a short yttria-stabilized zirconia solid electrolyte (YSZ) tube. Combining with cyclic voltammetry and potentiostatic electrolysis methods, green electrochemical preparation of Si from solid SiO_2 in $CaCl_2$ melt at 1173 K was studied via an experimental apparatus containing the novel integrated cell under complete carbon-free condition; the effect of electrolysis time on the morphology of the Si product was also investigated by scanning electron microscopy with energy dispersive X-ray spectroscopy (SEM-EDS). The results show that the morphology of the product obtained from potentiostatic electrolysis at a low overpotential (-1.6 V) undergoes an evolution from SiO_2 raw powder with different sizes to aggregates of the spherical particles and the small particles with partial reduction, and then to Si nuclei, and finally to Si wires or flakes. The morphology of electrolytic products has little relation with that of SiO_2 raw powder and may be controlled by applying different potentials. Furthermore, the longer the electrolysis time, the more the Si wires grow, and the higher the Si purity on the whole. It is feasible that the experimental apparatus without the sealed stainless steel reactor and any carbonaceous materials is used to prepare Si from solid SiO_2 in $CaCl_2$ melt, and release O_2 gas at the same time.

Keywords: Silica; Silicon; Calcium chloride; Green electrolysis; Zirconia solid electrolyte

I. INTRODUCTION

Silicon is the most basic functional material in the information, the new energy and the new materials industry. Two decades ago the introduction of FFC-Cambridge process has generated a continued interest in electrochemical preparation of Si from solid SiO_2 in $CaCl_2$ melt.[1–5] The researches focus not only on improving the purity of Si product, but also on the preparation of Si product with controllable morphology, structure, etc.[5–13] It is well known that Si is active at high temperatures, a sealable heat resistant stainless steel reactor had to be used to prevent the oxidation of Si in previous works,[2,4,5,9,11,13] and various carbonaceous materials were widely employed as electrodes or crucible container,[2–15] a large voltage was applied to electrolyze solid SiO_2.[5,9,14,15] In addition, an ion isolation membrane should be set up in electrochemical cell to avoid physical interference of the components in different electrode zones; however, it was difficult to choose a suitable material for the ion membrane at high temperatures. These practices not only lead to low efficiency of electrolysis due to electronic conduction in molten salt, and the release of unfriendly gases such as CO_x or even Cl_2, but also induce the side reaction on calcium reduction and the contamination of products by various components including stainless steel and potential impurities such as carbon and calcium.[5,16,17]

ZrO_2 doped with oxides such as Y_2O_3 or MgO is a kind of oxygen-ion-conducting solid electrolyte with good stability and strong resistance to melt at high temperatures.[18] In recent years, it has been used as solid oxide membrane (SOM) in the electrochemical preparation of various metals or intermetallic compound (e.g. Mg, Al, Ti, Ca, Ta, Fe, $CeNi_5$, Ti-Fe, $TiAl_3$, etc.) from respective metal oxides.[14,15,19–23] Furthermore, it is frequently used to construct an independent $O^{2-}|ZrO_2|Pt|O_2$(air) reference electrode (RE) with a flowing air at high temperatures for oxygen-related electrochemical studies.[18,24,25] The $O^{2-}|ZrO_2|Pt|O_2$(air) RE is essentially an O^{2-}/O_2 pair, which is generally considered to be responsive, stable, reversible and reproducible.[18,25] In view of the above applications, authors' research group constructed a novel integrated cell with $O^{2-}|ZrO_2|Pt|O_2$(air) RE by using a ZrO_2 solid electrolyte tube, which is simple and unique in structure and fabrication. The integrated cell has been successfully applied to electrochemical fundamental research in high-temperature melt.[26–28]

It is well known that solid SiO_2 is electronically insulating at high temperatures, the electroreduction of SiO_2 to Si (Eq. [1]) can occur only at three-phase interlines (3 PIs) of conductive current collector and solid SiO_2 cathode and molten salt (electrolyte):[17,29]

$$SiO_2(s) + 4e \rightarrow Si + 2O^{2-} \quad [1]$$

The generated Si nuclei may act as new current collectors due to their good conductivity. With the reduction, the Si nuclei continue to grow and evolve, and the 3 PIs extend until the SiO_2 is completely reduced. In this work, Si was attempted to prepare from solid SiO_2 in $CaCl_2$ melt at 1173 K in an experimental apparatus containing the novel integrated cell with $O^{2-}|YSZ|Pt|O_2$(air) RE constructed by yttria-stabilized zirconia solid electrolyte (YSZ) tube, and O_2 gas was released at the same time. The effect of electrolysis time on the morphology of the electrolytic Si was also investigated at a low overpotential. Herein the YSZ tube was used as the cell container, and also as the ion conducting but electron insulating membrane to electronically and physically isolate

working electrode (WE) and counter electrode (CE) or RE, which could improve electrolysis efficiency and avoid electrolysis of molten chloride salts at even high applied potentials.[21] It also provided a basal body integrating the CE with the RE. Moreover, compared with previous works,[2–15] the experimental apparatus contained neither sealable stainless steel reactor nor carbonaceous electrode or crucible, which could fundamentally eliminate their contamination to the electrolytic Si and the formation of CO_x gases, also avoid carbon entering molten salt to reduce current efficiency due to electronic conduction.

The goal of the present work is to demonstrate the use of the experimental apparatus with the novel integrated cell as a simple and convenient tool for green electrochemical preparation of contamination-free Si from solid SiO_2 in the laboratory, while we hope that the findings reported in the work will benefit similar studies of other high-temperature electrolytes and the future design of the industrial cell capable of continuous operation, and the selection, monitor, and control of the process variables for optimal production.

II. EXPERIMENTAL

A. *Materials Preparation*

SiO_2 and $CaCl_2$ used in this work were analytical pure grade reagents provided by Chinese Pharmaceutical Group Chemical Reagent Co., Ltd. The SiO_2 powder was loaded into a steel mold, cylinder samples were obtained by using 1.56 MPa pressure. Each cylinder sample was about 5 mm diameter, 10 mm height and 0.12 g mass. They were sintered for 4 h at 1673 K under air, which made them have certain porosity and strength. The $CaCl_2$ powder, used as the electrolyte, was dried under a vacuum of less than 133 Pa for 8 h at 473 K to dehydrate adequately.

B. *Integrated Cell and Electrodes*

The integrated cell consisted of an YSZ tube with a closed end and three electrodes including CE, RE and Mo-SiO_2 WE. The YSZ tube (inner diameter18 mm, outer diameter 20 mm and length 100 mm) contained 8 mol% Y_2O_3. After the YSZ tube was ultrasonically cleaned with alcohol, the porous annular Pt CE (area about 6.28 cm^2) and RE (area about 1.88 cm^2) were prepared according to the method provided in literature.[26,28] The Pt leads (diameter 0.5 mm and length 800 mm) for the RE and the CE were each protected in a thin double-bore alumina tube.

The Mo-SiO_2 WE was prepared as follows. The drill bit of 0.9 mm was used to punch the center of the sintered SiO_2 cylinder. One end of Mo wire (purity 99.99%, diameter 1 mm, length 800 mm), polished by a fine sandpaper (2000 mesh), was tightly coated with a thin single-bore alumina tube and slid for leaving a short length of bare wire through the central hole of the SiO_2 cylinder. The end of the bare wire was bent to prevent the SiO_2 cylinder from sliding into the molten salt during the process of lowering or electrolysis; the thin single-bore alumina tube covering the Mo wire tightened the upper end of the SiO_2 cylinder, which prevented the SiO_2 cylinder from moving up during the process of lowering.

C. *Experimental Method*

Figure 1 shows schematically the experimental apparatus used in this work. Since the YSZ tube was short to only 100 mm, in order to operate conveniently and isolate the atmosphere inside and outside the YSZ tube, the open end of the YSZ tube used as electrolytic cell was connected with an extended alumina tube (inner diameter 21 mm, outer diameter 25 mm and length 600 mm) by high-temperature cement. The preliminary experimental result showed that the joint between the YSZ tube and the alumina tube was well sealed after sintering at 1173 K and no leakage was found when it was immersed in water at room temperature. The thin double-bore alumina tube, covering the RE and the CE leads (Pt wires), was bound to the alumina tube with Cu wire (diameter 0.5 mm). The electrode leads were respectively fixed with thin Pt wire (diameter 0.3 mm) to the corresponding RE and CE on the outer surface of the YSZ tube. By means of the alumina tube, the integrated cell loading the dried $CaCl_2$ powder (about 12 g) was put into the constant temperature zone of a high-temperature furnace. The heating element of the furnace was SiC tube, the furnace tube (inner diameter 45 mm, length 100 cm) was alumina material and an S type thermocouple was used to measure temperature of the furnace. The furnace was heated from room temperature to 723 K at a rate of 3 K/min, and then continued to 1173 K at a rate of 4 K/min and held for 30 min. High purity argon (purity 99.999%, $O_2 \leq 1.5$ ppm), dried via a pair of the molecular sieves and the silica gel columns, was introduced into the YSZ tube with a flow rate of 10 mL/min throughout the experiment, while it was not until the experimental temperature was reached that the dried synthetic air (79% N_2, 21% O_2) with a flow rate of 300 mL/min was introduced into the furnace, that is outside the YSZ tube, to construct a $O^{2-}|YSZ|Pt|O_2(air)$ RE. All potentials (E) in this work referred to the potential relative to the $O^{2-}|YSZ|Pt|O_2(air)$ RE. Compared with the electrolytic cell in conventional crucible form, the amount of $CaCl_2$ powder used in the YSZ tube was very small, which was favorable to remove fully the moisture in the $CaCl_2$ during the process of heating, holding and pre-electrolysis.

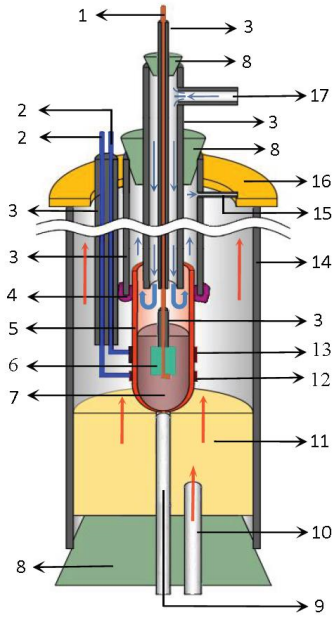

1-Mo wire;
2-Pt wire;
3- Al_2O_3 tube;
4-Cement;
5-YSZ tube;
6- Mo-SiO_2 WE;
7-$CaCl_2$ melt;
8-Rubber plug;
9-Type S thermocouple;
10-Inlet (air);
11-Porous Al_2O_3 block;
12-RE (Pt gauze);
13-CE (Pt gauze);
14- Al_2O_3 furnace tube;
15-Outlet (Ar);
16- Al_2O_3 cover;
17-Inlet (Ar).

Fig. 1 Experimental apparatus used in this work.

Electrochemical tests were conducted with a three-electrode method using an electrochemical workstation (model: IviumStat.h, made in Netherlands) connected to a computer. After holding the temperature, a Ni wire (purity 99.99%, diameter 0.5 mm) was used as cathode to pre-electrolyze for 90 min at -1.8 V. After the Ni wire was removed, the Mo-SiO_2 WE was slowly lowered from the furnace top to the above of the melt level, and then the melt level was determined by the open circuit potential method to ensure that the whole SiO_2 cylinder was immersed in the melt.[28] Electrochemical behavior of the Mo-SiO_2 WE was investigated by cyclic voltammetry (CV) method. Based on this test, the electroreduction of solid SiO_2 was studied at a lower overpotential by chronoamperometry (potentiostatic electrolysis) method.

The synthetic air in the furnace was cut off after the measurements were finished. The Mo-SiO_2 WE in the YSZ tube was lifted above the melt level and cooled to room temperature with the furnace under the protection of argon. The appearance of the YSZ tube was first observed with the naked eye. And each electrolyzed cylinder was soaked for 30 min in a beaker with a small amount of distilled water. One could observe whether gas bubbles were formed in the water, and then used a pH paper to detect the acidity and alkalinity of the water. The electrolytic products were further washed ultrasonically with distilled water for 3 min, and then dried for 20 h in the vacuum at 343 K. The dried cylinder sections were characterized by scanning electron microscopy (SEM, Nova NovaSEM400) with energy dispersive X-ray spectroscopy (EDS, INCA IE 350PentaFET X-3EDS). If necessary, the section of the Mo current collector was also observed under SEM-EDS. Since the mass of the SiO_2 cylinder was small to only 0.12 g, phase detection was not carried out by X ray diffraction (XRD) after electrolysis. To compare with the electrolytic products, morphology observation, composition analyses and phase detection for the SiO_2 raw powder and the sintered SiO_2 cylinder were conducted with SEM-EDS and XRD, respectively.

III. RESULTS AND DISCUSSION

A. *CV*

Figure 2 shows a typical cyclic voltammogram of the Mo-SiO_2 WE in $CaCl_2$ melt. A scan is performed with a rate of 50 mV/s in a potential range of -0.5 to -1.8 V. It is clear that, a reduction peak C_1 first appears. It can be noted that the potential (-0.73 V) of the peak C_1 is close to the theoretical potential (-0.75 V) of MoO_3 reduction to Mo,[30] indicating that the peak C_1 corresponds to the reduction of Mo^{6+} to Mo in the melt (Eq. [2]):[31]

$$Mo^{6+} + 6e \rightarrow Mo \qquad [2]$$

There are two reasons for the formation of Mo^{6+} in the melt. One reason is that, when the Mo-SiO_2 WE is lowered, the Mo wire reacts with the residual oxygen in argon at high temperatures to form a small amount of MoO_3 (melting point 1068 K, boiling point 1428 K), some of which volatilize and some adhere to the surface of Mo wire into the melt. Graphite electrode or crucible was often used in previous works,[2–15] which could protect Mo from oxidation by the atmosphere, hence no reduction peak of the Mo^{6+} was observed. The other is that a large oxidation current can be observed from Figure 2 when the potential scan is initially performed from -0.5 V, indicating that the Mo wire in the melt may have been electrochemically oxidized to Mo^{6+}. Obviously, the peak

A_1 with the potential of about -0.65 V corresponds to the oxidation of Mo to Mo^{6+}.

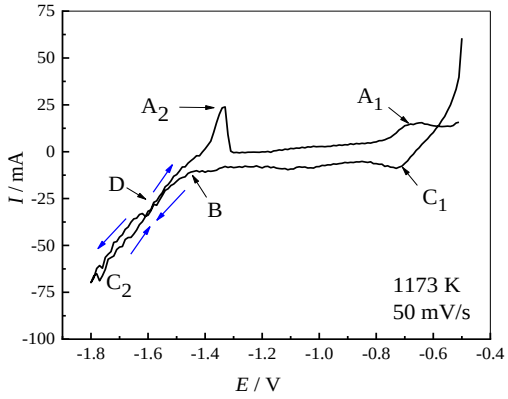

Fig. 2 Typical cyclic voltammogram of the Mo-SiO_2 WE in $CaCl_2$ melt (RE: O^{2-}|YSZ|Pt|O_2(air))

As the scan continues forward, the current changes little prior to the position B where the onset potential of a new peak C_2 is about -1.45 V. The peak C_2 is incomplete and most likely to correspond to the SiO_2 reduction. However, the reduction potential of SiO_2 at 1173 K is -1.77 V from thermodynamic theory calculation.[30] It is inferred that the onset potential of the peak C2 corresponds to SiO_2 reduction on the Mo to form an alloy with the Si activity of less than unity, which results in an advance of the SiO_2 reduction potential to -1.45 V. Figure 3 shows a SEM image of cross section of the Mo wire after potentiostatic electrolysis. The EDS analyses of relevant position points in Figure 3 are listed in Table I. As expected, a Si-Mo alloy layer formed at the edge of the Mo wire is found. As the position moves from the edge to the center of the Mo wire, Si content in the alloy decreases and Mo content increases, indicating that Si gradually alloyed with Mo from the surface to the center of the Mo wire. Inexplicably, the formation of alloy between Mo and Si was rarely noted in previous works.

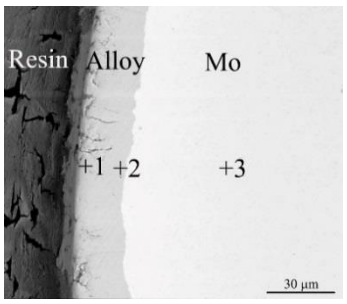

Fig. 3 SEM image of Mo wire section after potentiostatic electrolysis for 5 ks at 1173 K and -1.8 V (RE: O^{2-}|YSZ|Pt|O_2(air)).

Table I. EDS analyses of relevant position points in Figure 3.

Points	Atomic fraction / %	
	Mo	Si
1	14.35	85.65
2	22.57	77.43
3	100	-

A crossover of the forward and the reverse curve at the position D (around -1.60 V) is observed, indicating the increases of the total length of 3PIs and also the area of the Si/$CaCl_2$ interface where the new phase Si nuclei are generated.[2,29] Furthermore, the reoxidation part exhibits a sharp decrease in current after a peak A_2 which is typical of a stripping effect due to the depletion of the product reduced during the forward (negative) scan. Obviously, the A_2 with peak potential of -1.34 V can be attributed to the reoxidation of Si.

B. *Potentiostatic Electrolysis*

Under the experimental conditions, it was found that the SiO_2 could be reduced at -1.45 V according to Figure 2, and the crossover of the forward and the reverse curve occurred at -1.6 V. Therefore, the cross-potential of -1.6 V was used to electrolysis for 3 ks, 5ks and 6 ks, respectively. The preparation of Si and the change of its morphology from electrolysis of solid SiO_2 were studied by using the integrated cell in this experiment. Figure 4 shows the current curves with time for SiO_2 electrolysis at -1.6 V and 1173 K. It can be seen that the current curves are similar.

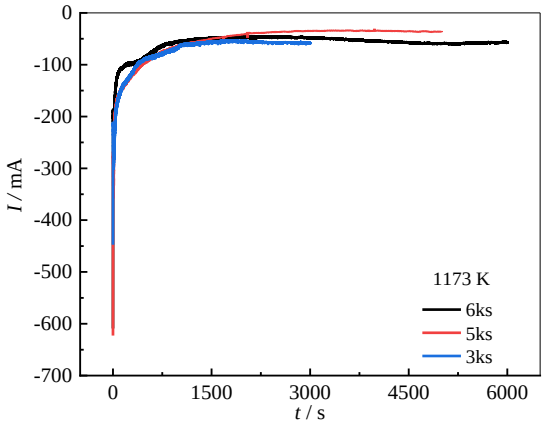

Fig. 4 Current curves with time for solid SiO_2 electrolysis in $CaCl_2$ melt at -1.6 V (RE: O^{2-}|YSZ|Pt|O_2(air)).

The YSZ tube cooled to room temperature was found to exhibit obvious moisture state on the outer surface position below the melt level in the YSZ tube after the electrolysis for different times, but no crack or melt leakage was observed with the naked eye. Moisture is a clear sign of water absorption of $CaCl_2$ penetrating into the YSZ membrane. It is tentatively speculated that the permeability of $CaCl_2$ enhanced in the inner surface of the YSZ tube in this work. This will be further explained later.

For each cylindrical sample soaked in the water after electrolysis for different times, no obvious bubble was observed, and the water showed neutral by detecting with PH paper, indicating that there was no Ca metal or Ca-Si alloy in the electrolytic products, which is consistent with the CV result. After further ultrasonic washing and drying, a brown product layer can be observed in the sections of the three cylinders with different electrolysis times, which is obviously different from white SiO_2 raw material. The present of brown color indicates that the SiO_2 has been electrolyzed to Si in this experiment.[29,32] It is believed that solid SiO_2 is reduced to Si at the cathode (Eq. [1]), the oxide ions produced from the solid structure migrate in the melt and solid electrolyte and are oxidized to O_2 gas at the anode outside the YSZ tube (Eq. [3]).

$2O^{2-} \rightarrow O_2 + 4e$ [3]

However, an obvious white layer could also be found in the outer region of the cylinder section far away from the Mo current collector for electrolysis time of 3 ks and 5 ks, respectively. An integral calculus for the current curve with electrolysis of 6 ks was performed. According to Faraday law, the reduction rate with electrolysis of 6 ks was only 54.4% in theory even if the current efficiency was assumed as 100%, indicating that the electroreduction of solid SiO_2 cylinders was also incomplete within the given time of 6ks due to small electrolysis current. It could be expected that whole SiO_2 cylinder was reduced to Si by an extension of the electrolysis time.

Here, the morphology and the composition of the brown products obtained were mainly analyzed with SEM-EDS detection, whereas the alloy formed on the Mo current collector and white unreduced layer were not considered.

The morphology of the SiO_2 raw powder and the sintered cylinder was first observed under SEM, as shown in Figure 5. The SiO_2 raw powder is loose (Figure 5(a)), the difference in the particle size is large and generally between 5–50 mm. The particles in cross-section of sintered cylinder become tight. The number of small particles increases, and they are easy to adhere on the surface of large particles (Figures 5(b) and 5(c)), indicating that some large particles of SiO_2 raw powder are crushed and become small after pressing and sintering. It can also be found that the particles experienced a slight softening-melting phenomenon after sintering and even adhere to each other slightly (Figure 5(c)), but they can still maintain their shapes with different sizes. Moreover, the SiO_2 raw powder and the sintered cylinder are found to be pure SiO_2 crystal phase by XRD and EDS detection (not shown here), and no change in the composition.

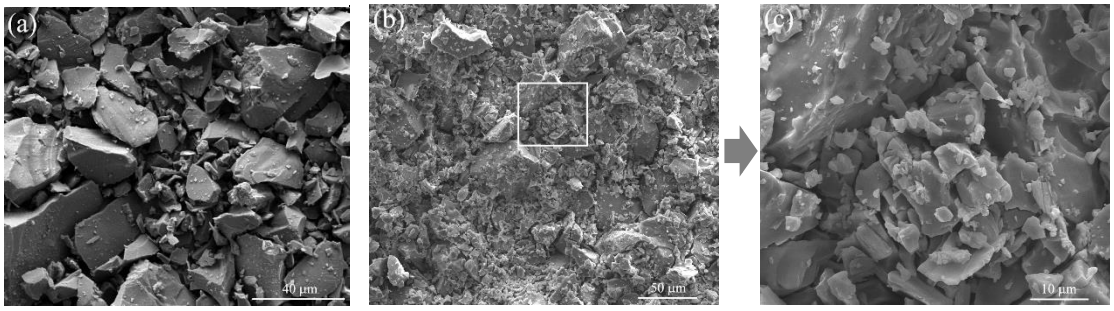

Fig. 5 SEM images of SiO_2 raw powder (a) and sintered cylinder section (b) and local magnification (c).

Figure 6 shows SEM images of the brown products from electrolysis for 3 ks. It can be found that the morphology is completely different compared with the sintered SiO_2 particles (Figures 5(b) or 5(c)). The brown products obtained are loose spongy particles (Figure 6(a)), most of them are large spherical particles with about 1 μm diameter at higher magnification (Figure 6(b)). Some large spherical particles aggregate with each other and some small particles within about 300 nm diameter are not uniformly gathered around the aggregates. Moreover, some beads with diameters of 100–300 nm or rod-like substances with less than 1.5 μm in length grow on the surface of some large spherical particles (Figure 6(b)). It can be inferred that large change of the morphology of the particles before and after electrolysis is attributed to the electroreduction of SiO_2 particles and the physicochemical interaction between the SiO_2 particles and the melt. And the morphology of electrolytic products has little relation with that of the sintered SiO_2 particles. The EDS analyses

of the relevant position points in Figure 6(b) are listed in Table II. The EDS detection (Table II) shows that Si content of each position in the electrolytic products in general is higher than that in the sintered SiO_2 particles before electrolysis, while O content in the spherical particles is higher than that in the small particles after electrolysis. Occasionally, a small amount of $CaCl_2$ or CaO is found. The $CaCl_2$ is the residue after washing, while the CaO is generated due to hydrolysis of $CaCl_2$ or during the electroreduction of SiO_2 and it can further react with solid SiO_2 to form an intermediate of $CaO{\cdot}SiO_2$.[5,28,33,34]

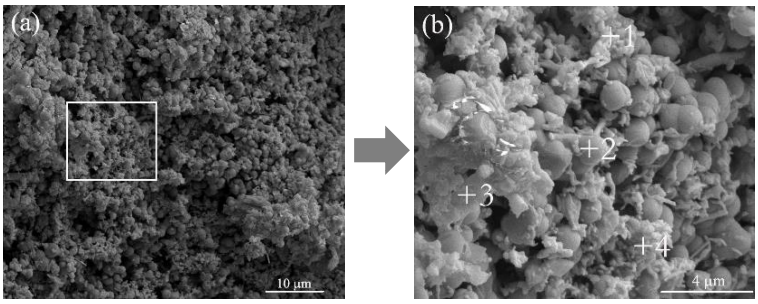

Fig. 6 SEM images of cylinder section after electrolysis for 3 ks (a) and local magnification (b).

Table II. EDS analyses of related position points in Figure 6(b).

Points	Atomic fraction / %		
	Si	Ca	O
1	69.80	-	30.20
2	49.17	-	50.83
3	86.42	-	13.58
4	66.80	5.87	27.32

The color change and the EDS analyses of the cylinder before and after electrolysis show that the large and the small particles evolved from the original SiO_2 powder have been partially reduced. As mentioned earlier, the partially reduced spherical particles and small particles, together with beads and rod-like substances, compose the aggregates; their distributions are also uneven in the aggregates. It can be considered that the beads and the rod-like substances with higher Si content grew from Si nuclei. The Si nuclei could be generated at -1.6 V, which seems to be consistent with the CV result. Combining with the 3 PIs theory on the electroreduction of solid SiO_2 in molten salt,[17,29] it is inferred that a conductive Si network has been initially formed in the aggregates (especially including small particles and rod-like substances), which can act as new network current collector to promote further reduction of solid SiO_2.

Figure 7 shows SEM images of brown products from electrolysis for 5 ks. Compared with Figure 6, the morphology of the products also changes greatly. Although the products are also composed of small particles and rod-like substances or wires, the diameter and the length of rod-like substances increase, and the number increases significantly. In contrast, the number of spherical particles with higher O content decreases significantly. Rod-like substances grow longitudinally on the surface of spherical particles, some of which continue to grow into wires;

some tend to merge into flakes. The rods or the wires are of varying diameter. The gaps in the products also increase obviously, indicating that the removal amount of O in the SiO_2 cylinder increases. The EDS analyses of the relevant position points in Figure 7(b) are listed in Table III. The EDS detection (see Tables II and III) shows that the main constituent in small particles or rod/wire-like substances is Si, and Si contents in some positions are even as high as 100 at%. By contrast, some near-spherical particles contain more unreduced SiO_2. It is known that many experiments[29,32,35,36] on the electroreduction of solid SiO_2 in molten salt were performed in a sealed stainless steel reactor with argon flow, and even with the use of carbonaceous electrode or crucible, the surface of the reduced Si was still found to cover with a thin layer (thickness around 10 nm) of amorphous SiO_2, which was generally attributed to slight oxidation of Si in Ar atmosphere at high temperatures or passivation during washing at room temperature, indicating that it is very difficult to obtain high purity Si with very low oxygen content only by electrolysis in Ar atmosphere.

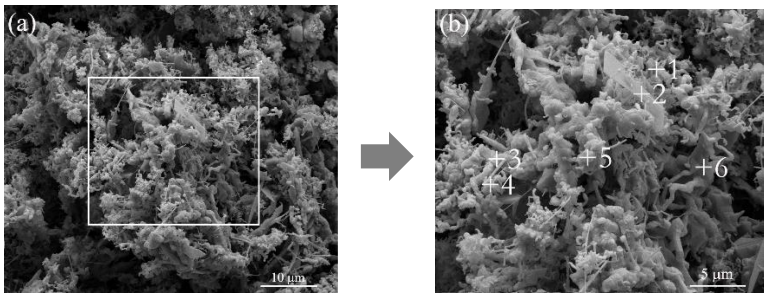

Fig. 7 SEM images of cylinder section after electrolysis for 5 ks (a) and local magnification (b).

Table III. EDS analyses of related position points in Figure 7(b).

Points	Atomic fraction / %			
	Si	Ca	O	Cl
1	64.23	3.65	29.26	2.86
2	81.97	-	18.03	-
3	100.00	-	-	-
4	64.84	6.00	29.17	-
5	79.74	-	20.26	-
6	100.00	-	-	-

In view of 3 PIs theory, combining with the morphology of the products from electrolysis for 3 ks, it can be speculated that the solid SiO_2 raw powder was spheroidized into new particles under the electrolysis and the physicochemical interaction between the SiO_2 particles and the melt, and then fine Si nuclei grew on the surface of spherical particles and formed Si network current collectors along with small particles with low oxygen content, and continued to grow longitudinally into rod-like substances, finally into Si wires or flakes. Meanwhile the network current collectors further extended until the original SiO_2 disappeared due to complete reduction.

Figure 8 shows SEM images of brown products from electrolysis for 6 ks. The morphology of the products (Figures 8(a) and 8(b)) is basically the same as that in Figure 7. It is mainly

composed of small particles, wires and flakes. The wires is considered to grow from the rod-like substances mentioned earlier, the difference in diameter between the two is small, but the longitudinal length of the former increases. It is believed that most of rod-like substances have grown into the wires, and there are some sites where the rod-like substances merge each other to form larger flakes under specific conditions (Figure 8(b)). The number of the spherical particles has been few, indicating further increase in reduction. The EDS sum spectrum (Figure 8(c)) shows that Si content in the brown products exhibited in Figure 8(b) is over 95 at% locally, and content of O or Ca is very low and could be further reduced if adequate washing. The Ca content is slightly higher than the O content, which may be due to error in the EDS detection or Cl not included. Combining with the above-mentioned detection on the electrolytic products soaked in the water, it can be concluded that no Ca metal or Ca-Si alloy was formed during the electrolysis. Furthermore, no Zr or Y from YSZ tube was found in the products, either. Therefore, under a complete carbon-free condition, the Si specimens with local high purity can be obtained in the YSZ tube (where the gas is under argon atmosphere) even if the gas outside the YSZ tube is under the air in this work, indicating that the YSZ tube can not only act as oxygen ion isolation membrane, but also has good atmosphere isolation function at high temperatures, which also proves that the joint part between the YSZ tube and the extended alumina tube has a good seal. It can be believed that the sealable stainless steel reactor and carbonaceous anode or crucible used in previous works[2–15] are not essential during the electroreduction of solid SiO_2 to Si. The experimental apparatus used in this work not only meets the requirement of preventing the oxidation of the active Si, but also eliminates fundamentally the potential contamination of the Si product caused by stainless steel reactor, carbon and even Ca metal or Ca-Si alloy, which provides a possibility to establish a green technique for preparation of high purity Si and the release of O_2 gas by electrolysis of solid SiO_2 in $CaCl_2$ melt. Moreover, the longer the electrolysis time, the looser the reduction products, the more and longer the Si wires, the higher the Si content. Of course, still there are several other potential contamination sources such as the alumina tube and the Mo wire electrode in this work. In order to prepare Si from solid SiO_2 without contamination-free in the $CaCl_2$ melt and obtain high purity Si in the succeeding work, referring to the related findings[4,16], it can be considered to replace the Al_2O_3 tube touching with SiO_2 cylinder with Si or SiO_2 tube, and to replace the Mo wire electrode with Si rod. It is also necessary for the electrolytic products to be cleaned fully.

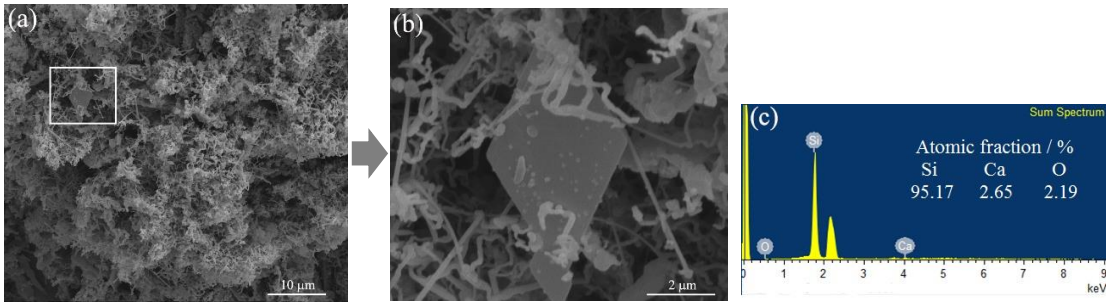

Fig. 8 SEM images (a) of cylinder section after electrolysis for 6 ks and local magnification (b) and its EDS sum spectrum(c). (The peak of unlabeled element in the sum spectrum is attributed to that of gold).

Noted the morphology of the Si product in this work is obviously different from that in the works of Zhao[14] and Lai et al[15] in $CaCl_2$ melt. They used SOM process with a two-electrode method and applied voltages (3.2–4 V) to electrolyze solid SiO_2 at above 1273 K. The Si particles, rather than the Si wires and flakes in this work, were obtained, which might be attributed to larger voltages and higher temperatures in their works. It is believed that the morphology of Si product may be controlled by applying different potentials. Furthermore, Ca metal or Ca-Si alloy could also be obtained at large voltages, which would adversely affect the electrochemical reduction of solid SiO_2.[29]

The stability of YSZ tube is also an important issue. Due to the different cell configuration, the moisture phenomenon appeared in this work cannot be observed in the works of Zhao[14] and Lai et al[15]. It is worth mentioning that the electrochemical behavior of Fe_2O_3 dissolved in $CaCl_2$-NaCl melt was studied by using the same cell as this work (except for the size of the YSZ tube).[28] Unlike this work, however, no moisture phenomenon was observed on the outer surface of the YSZ tube, and the $O^{2-}|ZrO_2|Pt|O_2$ (air) RE worked normally. A considerable number of researches on using the SOM process with a two-electrode method to prepare metals such as Mg, Si and Al from respective dissolved oxides show that the YSZ tube in molten halides presents a certain unstability.[37-41] The source of unstability lies in the leaching of stabilizer Y_2O_3 in solid solution, which induces the transformation of ZrO_2 from cubic to monoclinic phase, resulting in YSZ tube cracking or even breaking. Moreover, the electronic conductivity of the system exacerbates this unstability. From the point of view of the stability of YSZ tube, the content of dissolved SiO_2 or Al_2O_3 in the melt should not be too high[37,38]. It is also worth noting that the role of the dissolved CaO on YSZ stability seems contradictory in literature[38,40,41] , which may be attributed to the difference of the melt. However, the addition of Y_2O_3 or YF_3 to the melt was found to alleviate or completely prevent the YSZ tube degradation resulting from Y_2O_3 chemical leaching.[37-41] Combining these findings[37-41], the stability of YSZ tube in the melt can be preliminarily estimated in this work. It is well known that $CaCl_2$ exposed to air is easily hygroscopic at room temperature. The literature has shown that the $CaCl_2$ could penetrate into and remain in grain boundaries and the pores left in the ZrO_2 grains after Y_2O_3 leaching.[37,40] After the experiment, it is because of the hygroscopicity of the residual solidified $CaCl_2$ in the YSZ membrane that results in the moisture observed on the outer surface of the YSZ tube. Since the applied potential is small in the negative, the time is short at high temperature and the solubility of SiO_2 or $CaO{\cdot}SiO_2$ in the melt is small,[34] it can be understood that no crack or salt leakage in the YSZ tube was found. Referring to literature findings [37-41], some measures of modifying the melt, such as adding Y_2O_3 (YF_3 or YCl_3) or adjusting the optical basicity of oxides (SiO_2 and CaO), can be taken, and the direct touch of solid SiO_2 with YSZ tube is avoided during experiment, the degradation of YSZ tube in the $CaCl_2$-CaO melt will be expected to be alleviated or prevented completely in future preparation of high purity Si using the integrated cell.

IV. CONCLUSIONS

The novel integrated cell with $O^{2-}|YSZ|Pt|O_2$(air) RE and CE was constructed using short YSZ

tube connected with long extended alumina tube by high-temperature cement. In the experimental apparatus containing the integrated cell without stainless steel reactor and any carbonaceous materials, Si specimens with local high purity of over 95 at% was successfully obtained by electrolysis of solid SiO_2 in $CaCl_2$ melt at -1.6 V and 1173 K, and O_2 gas was simultaneously released. The CV test indicates that the reduction peak potential of $Mo^{6+} \rightarrow Mo$ is -0.73 V and the onset of reduction peak potential of $SiO_2 \rightarrow Si$ is -1.45 V in this work. The potentiostatic electrolysis at low overpotential shows that the morphology of the products underwent the evolution from SiO_2 raw powder with different sizes to particle aggregates with partial reduction, then Si nuclei formed on the surface of spherical particles, further growing longitudinally into rod-like substances, finally into Si wires or flakes. The morphology of electrolytic products has little relation with that of SiO_2 raw powder and may be controlled by applying different potentials. Furthermore, the longer the electrolysis time, the higher the purity of Si on the whole. The present work demonstrates the feasibility of green electrochemical preparation of Si from solid SiO_2 by using the experimental apparatus containing the novel integrated cell with $O^{2-}|YSZ|Pt|O_2(air)$ RE under complete carbon-free condition.

Acknowledgments

The authors acknowledge funding provided by the National Natural Science Foundation of China (Grant No. 51174148).

References

1. G. Z. Chen and D. J. Fray: *Nature*, 2000, vol. 407, pp. 361–364.
2. T. Nohira, K. Yasuda and Y. Ito: *Nat. Mater.*, 2003, vol. 2, pp. 397–401.
3. X. Jin, P. Gao, D. Wang, X. Hu and G. Z. Chen: *Angew. Chem. Int. Ed.*, 2004, vol. 43(6), pp. 733–736.
4. K. Yasuda, T. Nohira and Y. Ito: *J. Phys. Chem. Solids*, 2005, vol. 66, pp. 443–447.
5. J. Zhao, S. Lu, L. Hu and C. Li: *J. Energy Chem.*, 2013, vol. 22, pp. 819–825.
6. K. Yasuda, T. Nohira, K. Kobayashi, N. Kani, T. Tsuda and R. Hagiwara: *Energy Technol.*, 2013, vol. 1, pp. 245–252.
7. T. Homma T, N. Matsuo N, X. Yang, K. Yasuda, Y. Fukunaka and T. Nohira: *Electrochim. Acta*, 2015, vol. 179, pp. 512–518.
8. X. Yang, K. Yasuda, T. Nohira, R. Hagiwara and T. Homma: *Metall. Mater. Trans. B*, 2016, vol. 47, pp. 788–797.
9. W. Xiao, X. Jin and G. Z. Chen: *J. Mater. Chem. A*, 2013, vol. 1, pp. 10243–10250.
10. M. Zhong, X. Yang, K. Yasuda K, T. Homma and T. Nohira: *Metall. Mater. Trans. B*, 2018, vol. 49, pp. 341–348.
11. Y. Nishimura, T. Nohira, K. Kobayashi and R. Hagiwara: *J. Electrochem. Soc.*, 2011, vol. 158 (6), pp. E55–E59.
12. J. Yang, S. Lu, H. Ding, X. Zhang and S. Kan: *Chinese J. Inorg. Chem.*, 2010, vol. 26(10), pp. 1837–1843.
13. J. Zhao, J. Li, P. Ying, W. Zhang, L. Meng and C. Li: *Chem. Commun.*, 2013, vol. 49, pp. 4477–4479.
14. B. Zhao, X. Lu, X. Zou, S. Gu and W. Tao: *Materials Science and Technology*, 2011, vol. 19(2), pp. 113–117.
15. G. Lai, X. Zou, H. Cheng, K. Zheng, S. Li, S. Geng and X. Lu: *Journal of Functional Materials*, 2016, vol. 47(2), pp. 2177–2182.
16. K. Yasuda, T. Nohira, R. Hagiwara and Y. H. Ogata: *Electrochim. Acta*, 2007, vol. 53(1), pp. 106–110.

17. W. Xiao, X. Jin, Y. Deng, D. Wang, X. Hu and G. Z. Chen: *Chemphyschem*, 2006, vol. 7(8), pp. 1750–1758.
18. C. Z. Wang: *Solid Electrolyte and Chemical Sensors*, Metallurgical Industry Press, Beijing, 2000.
19. Y. Gao, X. Guo and K. Chou: *Acta Metall. Sin.*, 2006, vol. 42(1): 87–92.
20. X. Guan, S. Su，U. B. Pal and A. C. Powell: *Metall. Mater. Trans. B*, 2014, vol. 45, pp. 2138–2144.
21. X. Guan, U. B. Pal, Y. Jiang and S. Su: *J. Sustain. Metall.*, 2016, vol. 2, pp. 152–166.
22. A. Martin, D. Lambertin, J.-C. Poignet, M. Allibert, G. Bourges, L. Pescayre and J. Fouletier: *JOM*, 2003, vol. 55, pp. 52–54.
23. S. Li, X. Zou, K. Zheng, X. Lu, Q. Xu, C. Chen and Z. Zhou: *J. Alloy. Compd*., 2017, vol. 727, pp. 1243–1252.
24. S. C. Britten and U. B. Pal: *Metall. Mater. Trans. B*, 2000, vol. 31, pp. 733-753.
25. C. Mallika, O. M. Sreedharan and R. Subasri: *J. Eur. Ceram. Soc*., 2000, vol. 20, pp. 2297–2313.
26. Y. Gao, C. Hong and C. Yang: *J. Electrochem. Soc.*, 2015, vol. 162(14), pp. E362–E369.
27. Y. Gao, C. Yang, C. Zhang, Q. Qin and G. Z. Chen: *Phys. Chem. Chem. Phys.*, 2017, vol. 19, pp. 15876–15890.
28. H. Hu,Y. Gao,Y. Lao, Q. Qin, G. Li and G. Z. Chen: *Metall. Mater. Trans. B*, 2018, vol. 49(5), pp. 2794–2808.
29. W. Xiao, X. Jin, Y. Deng, D. Wang and G. Z. Chen: *J. Electroanal. Chem.*, 2010, vol. 639, pp. 130–140.
30. http://www.factsage.com/. Accessed 20 Nov 2020.
31. Ine Vanmoortel, Joost De Strycker, Eduard Temmerman and Annemie Adriaens: *Ceramics - Silikáty*, 2008, vol. 52(1), pp.1–7.
32. E. Ergül, İ. Karakaya and M. Erdoğan: *J. Alloy. Compd*., 2011, vol. 509(3), pp. 899-903.
33. K. Yasuda, T. Nohira, R. Hagiwara and Y. H. Ogata: *J. Electrochem. Soc.*, 2007, vol. 154(7), pp. E95–E101.
34. W. Xiao, X. Wang, H. Yin, H. Zhu, X. Mao and D. Wang: *RSC Adv.*, 2012, vol. 2(19), pp. 7588–7593.
35. W. Weng and W. Xiao: *ACS Appl. Energy Mater*., 2019, vol. 2(1), pp. 804–813.
36. S. K. Cho, Fu-Ren F. Fan and A. J. Bard: *Electrochim. Acta*, 2012, vol. 65, pp. 57–63.
37. J. Xu, Brian Lo, Y. Jiang, U. Pal and S. Basu: *J. Eur. Ceram. Soc*., 2014, vol. 34, pp. 3887–3896.
38. J. Guo, T. Villalon, U. Pal and S. Basu: *J. Am. Ceram. Soc*., 2018, vol. 101, pp. 3605-3616.
39. A. Martin, J. C. Poignet, J. Fouletier, M. Allibert, D. Lambertin and G. Bourge`s: *J. Appl. Electrochem.*, 2010, vol. 40, pp.533–542.
40. A Mukherjee, N Campagnol, JV Dyck, J Fransaer and B Blanpain: *J. Am. Ceram. Soc.*, 2015, vol. 98, pp. 972–981.
41. S. Su, U. Pal and X. Guan: *J. Electrochem. Soc.*, 2017, vol. 164, pp. F248–F255.

Table captions:

Table I. EDS analyses of relevant position points in Figure 3.

Table II. EDS analyses of related position points in Figure 6(b).

Table III. EDS analyses of related position points in Figure 7(b).

Figure captions:

Fig. 1 Experimental apparatus used in this work.

Fig. 2 Typical cyclic voltammogram of the Mo-SiO_2 WE in $CaCl_2$ melt (RE: O^{2-}|YSZ|Pt|O_2(air))

Fig. 3 SEM image of Mo wire section after potentiostatic electrolysis for 5 ks at -1.8 V (RE: O^{2-}|YSZ|Pt|O_2(air)).

Fig. 4 Current curves with time for solid SiO_2 electrolysis in $CaCl_2$ melt at -1.6 V (RE: O^{2-}|YSZ|Pt|O_2(air)).

Fig. 5 SEM images of SiO_2 raw powder (a) and sintered cylinder section (b) and local magnification (c).

Fig. 6 SEM images of cylinder section after electrolysis for 3 ks (a) and local magnification (b).

Fig. 7 SEM images of cylinder section after electrolysis for 5 ks (a) and local magnification (b).

Fig. 8 SEM images (a) of cylinder section after electrolysis for 6 ks and local magnification (b) and its EDS sum spectrum(c). (The peak of unlabeled element in the sum spectrum is attributed to that of gold).

546

547

548 **Table I. EDS analyses of relevant position points in Figure 3.**

Points	Atomic fraction / %	
	Mo	Si
1	14.35	85.65
2	22.57	77.43
3	100	-

549

550

551

552 **Table II. EDS analyses of related position points in Figure 6(b).**

Points	Atomic fraction / %		
	Si	Ca	O
1	69.80	-	30.20
2	49.17	-	50.83
3	86.42	-	13.58
4	66.80	5.87	27.32

553

554

555

556 **Table III. EDS analyses of related position points in Figure 7(b).**

Points	Atomic fraction / %			
	Si	Ca	O	Cl
1	64.23	3.65	29.26	2.86
2	81.97	-	18.03	-
3	100.00	-	-	-
4	64.84	6.00	29.17	-
5	79.74	-	20.26	-
6	100.00	-	-	-

557

558

559